frontiers | Frontiers in Astronomy and Space Sciences

TYPE Original Research
PUBLISHED 04 December 2024
DOI 10.3389/fspas.2024.1505560

Check for updates

OPEN ACCESS

EDITED BY
Armen Sedrakian,
University of Wrocław, Poland

REVIEWED BY
Praveen C. Srivastava,
Indian Institute of Technology Roorkee, India
Charalampos Moustakidis,
Aristotle University of Thessaloniki, Greece

*CORRESPONDENCE
G. F. Burgio,
fiorella.burgio@ct.infn.it

RECEIVED 03 October 2024
ACCEPTED 28 October 2024
PUBLISHED 04 December 2024

CITATION
Burgio GF, Das HC and Vidaña I (2024) The nuclear symmetry energy and the neutron skin thickness in nuclei.
Front. Astron. Space Sci. 11:1505560.
doi: 10.3389/fspas.2024.1505560

COPYRIGHT
© 2024 Burgio, Das and Vidaña. This is an open-access article distributed under the terms of the Creative Commons Attribution License (CC BY). The use, distribution or reproduction in other forums is permitted, provided the original author(s) and the copyright owner(s) are credited and that the original publication in this journal is cited, in accordance with accepted academic practice. No use, distribution or reproduction is permitted which does not comply with these terms.

The nuclear symmetry energy and the neutron skin thickness in nuclei

G. F. Burgio*, H. C. Das and I. Vidaña

INFN Sezione di Catania, Department of Physics and Astronomy, Università di Catania, Catania, Italy

Introduction: We investigate possible correlations between the stiffness of the symmetry energy at saturation density, the so-called L parameter, and the neutron skin thickness of ^{48}Ca and ^{208}Pb, for which the recent measurements from the CREX and PREX I + II experiments at the Thomas Jefferson Laboratory became available.

Methods: We choose an ensemble of nucleonic equations of state (EoS) derived within microscopic (BHF, Variational, AFDMC) and phenomenological (Skyrme, RMF, DD-RMF) approaches. They are all compatible with the laboratory nuclear collisions data and with current observations of neutron stars (NS) mass and the tidal polarizability of a 1.4 $M_\odot$ NS, as deduced from the GW170817 event.

Results: We find some degree of correlation between the L parameter and the neutron skin thickness whereas a much weaker correlation does exist with the tidal polarizability and the symmetry energy at saturation density. However, some EoS which are able to explain the CREX experimental data, are not compatible with the PREX I + II data, and viceversa.

Conclusion: We confirm the results previously obtained with a different set of EoS models, and find a possible tension between the experimental data and the current understanding of the nuclear EoS.

KEYWORDS

neutron star, equation of state, many-body methods of nuclear matter, neutron skin thickness, CREX, PREX I + II

1 Introduction

The nuclear symmetry energy plays a major role on the structure of neutron-rich finite nuclei as well as on the bulk properties of neutron stars (Li et al., 2014; Baldo and Burgio, 2016). In the past decades, several laboratory experiments (Russotto et al., 2023) have been performed in order to investigate the symmetry energy in finite nuclei, e.g., measurements of the nuclear masses (Möller et al., 2012), the nuclear dipole polarizability (Roca-Maza et al., 2015), the giant and pygmy dipole resonance energies (Klimkiewicz et al., 2007; Carbone et al., 2010), isobaric analog states (Danielewicz and Lee, 2014), and the neutron skin thickness (Adhikari et al., 2021; 2022). Several neutron stars (NS) properties are sensitive to the symmetry energy, e.g., its internal composition, the crust-core transition density and therefore the crust thickness, and the presence of fast direct URCA neutrino processes which regulate NS cooling (Yakovlev and Pethick, 2004; Burgio et al., 2021).

The symmetry energy is directly related to the more general and comprehensive task of the study of the equation of state (EoS), which plays a major role in nuclear structure studies, analysis of the heavy-ion collision dynamics, and the physics of

compact objects (Oertel et al., 2017; Burgio and Fantina, 2018). The central density likely reached in NS interiors is about one order of magnitude larger than the nuclear saturation density, and this poses serious problems in theoretical astrophysics, because a correct theory of nuclear interactions for highly dense matter should be derived from the quantum chromodynamics (QCD). The well-known sign problem of lattice QCD still bars access to the high-density EoS, and therefore, models extracted from the nuclear many-body theory are required in order to build the EoS. Predictions have to be tested both in terrestrial laboratories, and in astrophysical observations. The most promising NS observables are the mass and radius; as far as the masses are regarding, the ones of several NSs are known with good precision (Lattimer, 2012; Demorest et al., 2010; Antoniadis et al., 2013; Fonseca et al., 2016; Cromartie et al., 2019; Romani et al., 2022), while the information on their radii (Özel and Freire, 2016; Guillot et al., 2013) has been improved thanks to the combined observations of NICER (Riley et al., 2019; Miller et al., 2019) and Advanced LIGO and Virgo collaborations, with the detection of gravitational waves emitted during the GW170817 NS merger event (Abbott et al., 2017; Abbott et al., 2018; Abbott et al., 2019). This event has provided us with important new information on the NS mass and radii by means of the measurement of the tidal deformability (Hartle, 1967; Flanagan and Hinderer, 2008), thus deducing upper and lower limits on it (Abbott et al., 2018; Radice et al., 2018). Further constraints on mass and radius have been recently reported by NICER for PSR J1231-1411, having mass $M = 1.04^{+0.05}_{-0.03} M_\odot$ (Salmi et al., 2024).

In this paper, we concentrate on the study of the neutron skin thickness δR in neutron-rich nuclei, such as ^{208}Pb and ^{48}Ca, which has long been recognized as being strongly dependent on the slope of the symmetry parameter L. Novel data on ^{208}Pb (PREX-I and PREX-II) (Adhikari et al., 2021) and ^{48}Ca (CREX) (Adhikari et al., 2022) with direct measurements consisting of parity-violating and elastic electron scattering technique (Horowitz et al., 2001), recently became available from the Thomas Jefferson Laboratory. Correlations between the neutron skin thickness, symmetry parameters, and NS observables like the radius of $1.4M_\odot$ and tidal polarizability have been widely analyzed, see, e.g., (Lattimer, 2023), and references therein.

In our previous paper (Burgio and Vidaña, 2020), we studied those kind of correlations by choosing a set of EoS based on microscopic methods and phenomenological approaches, and discussing their behaviour with respect to the PREX-I experimental data, which were the available ones at that time. Now, we would like to elaborate more on that analysis, taking into account the recent PREX-II (Adhikari et al., 2021) and CREX data (Adhikari et al., 2022). Moreover, we now choose a set of equations of state EoS which are compatible with the NS data on the highest observed mass $M > 2.14^{+0.10}_{-0.09} M_\odot$ and tidal polarizability of a 1.4 $M_\odot$, $\Lambda_{1.4} = 190^{+390}_{-120}$. This way, we should be able to improve our study on the possible correlations among observational quantities and properties of nuclear matter close to saturation.

The paper is organized as follows. In Section 2 we illustrate some basic properties of the EoS adopted in this work, along with the criteria selection for the choice of the optimal EoS. The laboratory and observational constraints on the nuclear EoS are presented in Section 3. The neutron skin thickness is discussed in Section 4, and conclusions are drawn in Section 5.

2 The nuclear equation of state

The composition of high density nuclear matter currently represents one of the most intriguing issues in theoretical physics, and several and diverse predictions have been proposed thus far (Burgio et al., 2021). The description of the extreme density conditions can include different scenarios, e.g., a purely nucleonic one characterized by a large neutron-proton asymmetry, or hyperonic matter or a hadron-quark phase transition. All those issues suffer of drawbacks that the current experimental data, either heavy-ion collisions in terrestrial laboratories or NS observations, cannot solve. In this work, we assume that nucleons are the most relevant degrees of freedom.

Theoretical approaches to determine the nuclear EoS are usually classified in microscopic and phenomenological ones. The interested reader is referred to recent reviews (Burgio and Fantina, 2018; Burgio et al., 2021); in this paper, we skip details and summarize the main features of the adopted methods. For the microscopic approaches, we adopt several EoS derived in the Brueckner–Hartree–Fock (BHF) theory (Baldo, 1999), which is based on the use of realistic two- and three-body forces (TBF), derived from meson-exchange theory (Machleidt et al., 1987; Nagels et al., 1978) and describe correctly the nucleonic phase shifts and the properties of the deuteron. For the TBF we use the phenomenological Urbana model (Pudliner et al., 1995; 1997; Baldo et al., 1997), and a microscopic TBF (Grangé et al., 1989; Baldo et al., 1997; Zuo et al., 2002; Li et al., 2008; Li and Schulze, 2008). We adopt as nucleon-nucleon potentials the Bonn B (Machleidt et al., 1987; Machleidt, 1989), the Nijmegen 93 (Nagels et al., 1978; Stoks et al., 1994), and the Argonne V_{18} (Wiringa et al., 1995), which are supplemented by microscopic TBF and labeled in the following as BOB, N93 and V18. The Urbana model has been used with the Argonne V_{18} potential and is labeled as UIX. The explicit inclusion of the quark-gluon degrees of freedom in the construction of a potential model has been performed in Ref. (Baldo and Fukukawa, 2014; Fukukawa et al., 2015), in which case two different EoS versions labeled respectively as FSS2CC and FSS2GC in Table 1 have been obtained. Besides BHF EoS, in this paper we exploit the often-used results of the relativistic Dirac-BHF method (DBHF) (Gross-Boelting et al., 1999), which employs the Bonn A potential, the variational APR EoS (Akmal et al., 1998) based on the V_{18} potential, and the so-called CBF-EI model, obtained within the correlated basis function approach (Benhar and Lovato, 2017), using a realistic nuclear Hamiltonian with the Argonne V6' (Wiringa and Pieper, 2002) and the Urbana IX nuclear potentials as TBF. For completeness, we also include in our set a parametrization of the Auxiliary Field Diffusion Monte Carlo (AFDMC) calculation (Gandolfi et al., 2010).

The philosophy of the phenomenological approaches is quite different from the one characterizing microscopic methods. In fact, they are based on effective interactions that are built to describe finite nuclei in their ground state, and therefore, predictions at high isospin asymmetries and density have to be taken with care (Stone and Reinhard, 2007). Among the most used ones, we mention Skyrme interactions (Vautherin and Brink, 1972) and relativistic mean-field (RMF) models (Boguta and Bodmer, 1977). In this work, we use a set of modern Skyrme EoS, which are listed in Table 1; in particular we mention the SLy0-SLy10 (Chabanat, 1995) and

TABLE 1 Saturation properties predicted by the considered EoSs. Experimental nuclear parameters and observational data are listed for comparison. The references in the lower part of the table are labeled as [a] (Margueron et al., 2018); [b] (Shlomo et al., 2006); [c] (Piekarewicz, 2010); [d] (Burgio and Fantina, 2018); [e] (Burgio et al., 2021); [f] (Abbott et al., 2018); and [g] (Cromartie et al., 2019). See text for details.

Model class	EoS	ρ_0[fm^{-3}]	$-E_0$[MeV]	K_0[MeV]	S_0[MeV]	L[MeV]	$\Lambda_{1.4}$	$M_{max}[M_\odot]$
Microscopic	BOB	0.170	15.40	238	33.70	70.00	570	2.50
	V18	0.178	13.90	207	32.30	67.00	440	2.36
	N93	0.185	16.10	229	36.50	77.00	473	2.25
	UIX	0.171	14.90	171	33.50	61.00	309	1.96
	FSS2CC	0.157	16.30	219	31.80	52.00	295	1.94
	FSS2GC	0.170	15.60	185	31.00	51.00	262	2.08
	DBHF	0.181	16.20	218	34.40	69.00	681	2.31
	APR	0.159	15.90	233	33.40	51.00	250	2.19
	CBF-EI	0.160	10.90	240	30.00	68.00	501	2.47
	AFDMC	0.160	16.00	239	31.30	60.00	256	2.20
Skyrme	Rs	0.158	15.05	248	30.83	86.41	910	2.27
	SGI	0.155	15.89	265	28.35	63.85	714	2.31
	SLy0	0.160	16.01	226	31.40	45.37	315	2.06
	SLy1	0.161	15.98	233	32.59	48.88	314	2.06
	SLy2	0.161	15.92	235	32.39	48.84	318	2.06
	SLy3	0.161	15.96	233	32.12	45.56	295	2.05
	SLy4	0.160	15.97	232	31.85	45.38	309	2.06
	SLy5	0.161	15.98	232	32.70	50.34	328	2.07
	SLy6	0.159	15.92	230	31.21	45.21	334	2.09
	SLy7	0.159	15.90	233	32.41	48.11	337	2.09
	SLy8	0.161	15.96	233	32.51	45.36	316	2.06
	SLy9	0.151	15.79	229	32.12	55.37	513	2.23
	SLy10	0.156	15.90	232	32.19	39.24	262	2.04
	SLy230a	0.160	15.98	230	31.88	43.99	340	2.16
	SkI4	0.160	16.15	239	29.38	59.34	581	2.29
	SkMP	0.157	15.57	230	29.70	69.70	666	2.19
	SkO	0.161	15.78	228	32.19	79.92	656	2.10
	SkO′	0.160	15.73	222	32.10	69.68	465	2.00
	SkT4	0.159	15.95	235	35.23	93.48	919	2.23
	SkT5	0.164	15.99	201	37.60	100.3	807	2.08
	BSk20	0.160	16.04	241	30.00	37.40	328	2.18

(Continued on the following page)

TABLE 1 (*Continued*) Saturation properties predicted by the considered EoSs. Experimental nuclear parameters and observational data are listed for comparison. The references in the lower part of the table are labeled as [a] (Margueron et al., 2018); [b] (Shlomo et al., 2006); [c] (Piekarewicz, 2010); [d] (Burgio and Fantina, 2018); [e] (Burgio et al., 2021); [f] (Abbott et al., 2018); and [g] (Cromartie et al., 2019). See text for details.

Model class	EoS	ρ_0[fm^{-3}]	$-E_0$[MeV]	K_0[MeV]	S_0[MeV]	L[MeV]	$\Lambda_{1.4}$	$M_{max}[M_\odot]$
	BSk25	0.158	15.99	236	29.00	36.90	545	2.22
	BSk26	0.159	16.03	240	30.00	37.50	332	2.18
RMF	SINPA	0.151	16.00	204	31.24	54.01	586	2.00
	SINPB	0.150	16.04	206	33.92	71.47	623	1.99
	GL97	0.152	15.56	226	32.10	88.55	600	2.00
	BigApple	0.155	16.34	226	31.33	39.88	796	2.62
	BSR8	0.148	16.04	233	31.19	60.60	792	2.05
	BSR9	0.148	16.07	234	31.68	64.07	793	2.04
	FSUGarnet	0.153	16.23	229	30.89	53.85	740	2.12
	FSUGZ03	0.148	16.07	234	31.61	64.17	794	2.04
	G2*	0.153	15.95	213	30.29	69.43	692	2.05
	IUFSU	0.160	16.70	241	31.88	49.57	602	2.00
	G3	0.148	16.02	244	30.20	45.34	461	2.00
	IOPB-I	0.149	16.10	222	33.30	63.54	681	2.15
	NITR	0.155	16.32	224	31.51	43.46	683	2.36
DD-RMF	DD	0.148	16.50	239	32.58	58.73	750	2.43
	DD2	0.148	16.02	240	32.03	58.00	753	2.44
	DD-ME1	0.152	16.23	245	34.13	58.38	704	2.46
	DD-ME2	0.152	16.14	251	33.39	54.25	766	2.50
	TW-99	0.152	16.10	239	33.18	58.40	446	2.10
	Exp.	~0.14 – 0.17	~15 – 17	220 – 260	28.5 – 34.9	30 – 87	70 – 580	$> 2.14^{+0.10}_{-0.09}$
	Ref.	[a]	[a]	[b], [c]	[d], [e]	[d], [e]	[f]	[g]

SLy230a (Chabanat et al., 1997; 1998) of the Lyon group, and the BSk20, BSk25 and BSk26 of the Brussels group (Potekhin et al., 2013; Goriely et al., 2013), the latter ones being unified EoS constructed on the basis of the energy-density functional theory. A complementary approach is given by RMF models, which are based on effective Lagrangian densities. The interaction between baryons is described in terms of meson exchanges, which are regulated by coupling constants of nucleons with mesons, and are usually fixed by fitting the bulk properties of nuclear matter as well as masses and radii of finite nuclei. In this work, we consider two types of RMF models: models with density-dependent coupling constants labeled DD-RMF (Nikšić et al., 2002; Typel and Wolter, 1999; Xia et al., 2022) and RMF models with fixed coupling strength (Mondal et al., 2016; Fattoyev et al., 2020; Das et al., 2021; Dhiman et al., 2007; Chen and Piekarewicz, 2015; Kumar et al., 2006; Sulaksono and Mart, 2006; Fattoyev and Piekarewicz, 2010; Kumar et al., 2017; Kumar et al., 2018; Routaray et al., 2023).

The main properties of the chosen EoS at saturation density are listed in Table 1. We notice that, whereas the saturation properties of the phenomenological models are within the empirical range, some microscopic EoS are marginally compatible with it. The reason is that the parameters of the phenomenological models are fitted on the saturation properties, while they are a prediction in the case of microscopic calculations, and those depend both on the many-body approach and the choice of the employed forces. For instance, the V18 EoS predicts a slightly too low saturation energy E_0 and compressibility K_0, which is mainly due to the inclusion of a particular TBF (Li et al., 2008). We stress that a complete ab-initio theory of TBF is not available yet.

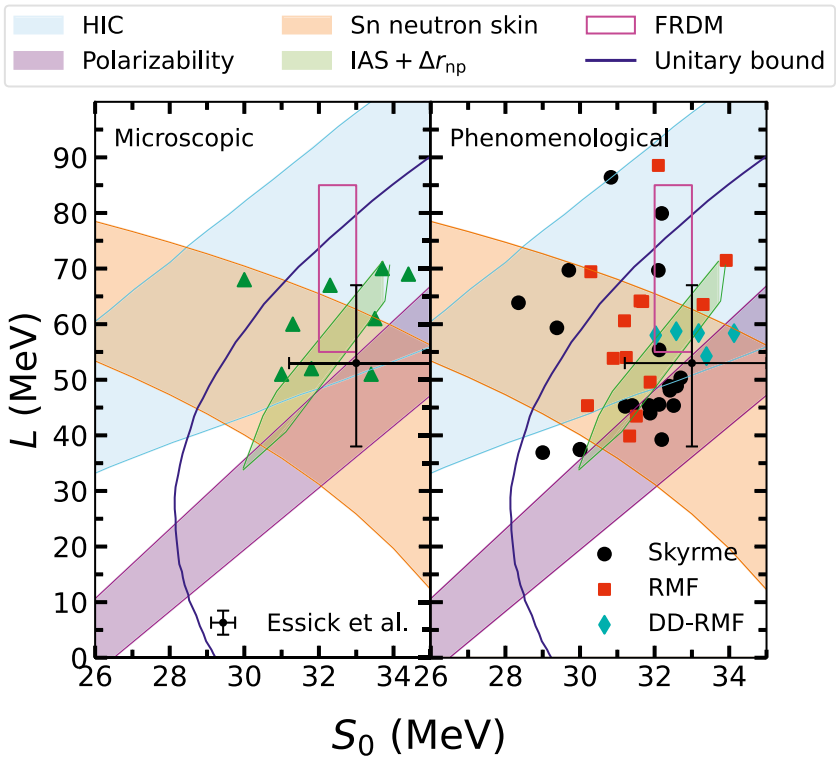

FIGURE 1
Symmetry energy slope L vs. the symmetry energy at saturation S_0. See text for details on the experimental data.

For completeness, we remind that the above mentioned methods are suited for describing the homogeneous component of the nuclear matter EoS, and that at densities $\rho < \rho_t \approx 0.08$ fm^{-3}, clusters have to be included for the description of the NS crust. For that, we use the well-known Negele-Vautherin EoS (Negele and Vautherin, 1973) in the density range (0.001 fm^{-3} $< \rho <$ 0.08 fm^{-3}), and the ones by Baym-Pethick-Sutherland (Baym et al., 1971) and Feynman-Metropolis-Teller (Feynman et al., 1949) for densities $\rho < 0.001$fm^{-3} typical of the outer crust.

2.1 Criteria for the selection of the EoS

The most important criterium for selecting the EoS is to check its behaviour with respect to the saturation properties of nuclear matter. In fact, around saturation density ρ_0 and isospin asymmetry $\delta \equiv (N-Z)/(N+Z) = 0$ [being $Z(N)$ the number of protons (neutrons)], the energy per particle of asymmetric nuclear matter $E(\rho,\delta)$ see Equations 1–3 can be expanded as a function of density and isospin asymmetry, and the coefficients are given by a set of few isoscalar (E_0, K_0) and isovector (S_0, L, K_{sym}) parameters (see Equations 4–7), which can be constrained by nuclear experiments. The expansion reads.

$$E(\rho,\delta) = E_{\rm SNM}(\rho) + E_{\rm sym}(\rho)\,\delta^2, \tag{1}$$

$$E_{\rm SNM}(\rho) = E_0 + \frac{K_0}{2}x^2, \tag{2}$$

$$E_{\rm sym}(\rho) = S_0 + Lx + \frac{K_{\rm sym}}{2}x^2, \tag{3}$$

where $x \equiv (\rho-\rho_0)/3\rho_0$, E_0 is the energy per particle of symmetric nuclear matter (SNM) at ρ_0, K_0 the incompressibility and $S_0 \equiv E_{sym}(\rho_0)$ is the symmetry energy coefficient at saturation, defined as

$$K_0 \equiv 9\rho_0^2 \frac{d^2 E_{\rm SNM}}{d\rho^2}(\rho_0), \tag{4}$$

$$S_0 \equiv \frac{1}{2}\frac{\partial^2 E}{\partial \delta^2}(\rho_0, 0) \tag{5}$$

The density dependence of the symmetry energy around saturation is characterized by the parameters L and K_{sym}, which are expressed as.

$$L \equiv 3\rho_0 \frac{dE_{\rm sym}}{d\rho}(\rho_0), \tag{6}$$

$$K_{sym} \equiv 9\rho_0^2 \frac{d^2 E_{\rm sym}}{d\rho^2}(\rho_0). \tag{7}$$

In Table 1, we list the saturation properties of the various considered EoSs, and compare them with available experimental data. Measurements of nuclear masses (Audi et al., 2003) and density distributions (de Vries et al., 1987) yield the saturation point $E_0 = -16 \pm 1$ MeV and $\rho_0 = 0.14 - 0.17$ fm^{-3}, whereas the value of K_0 can be extracted from the analysis of isoscalar giant monopole resonances in heavy nuclei, reporting $K_0 = 240 \pm 10$ MeV (Colò et al., 2004) or $K = 248 \pm 8$ MeV (Piekarewicz, 2004), in agreement with the low

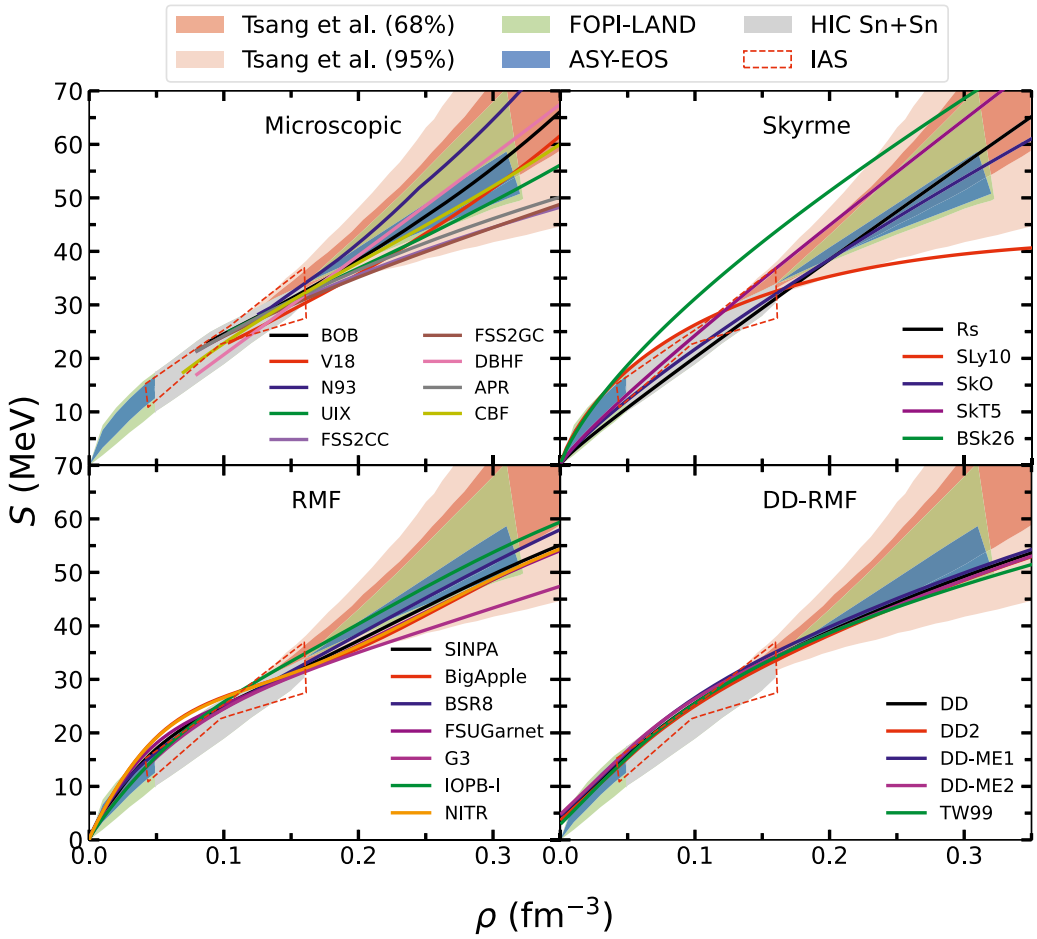

FIGURE 2
Symmetry energy vs. the nucleon density ρ. See text for details.

value of K_0 found in heavy ion collision experiments (Fuchs et al., 2001). We also notice that, whereas S_0 is more or less well established (≈30 MeV), the values of L (30 MeV < L < 87 MeV), is still quite uncertain (Reed, B. T., Fattoyev, F. J., Horowitz, C. J., and Piekarewicz, J., 2021; Essick et al., 2021; Lattimer, 2023). Also K_{sym} (−400 MeV < K_{sym} < 100 MeV) is poorly constrained (Tews et al., 2017; Zhang et al., 2017).

Besides the laboratory data, we also exploit astrophysical observation of NS. A very important constraint to be fulfilled by the different EoS is the value of the maximum NS mass, which has to be compatible with the observational data (Demorest et al., 2010; Antoniadis et al., 2013; Fonseca et al., 2016), in particular, the recent lower limit $M_{\max} > 2.14 \pm 0.1\ M_\odot$ (Cromartie et al., 2019). The GW detection by Advanced LIGO and Advanced Virgo (Abbott et al., 2017; Abbott et al, 2018; Abbott et al., 2019) of the GW170817 event put strong constraints on the so-called tidal polarizability Λ (Hinderer, 2008; Hinder, 2009; Hinderer et al., 2010), which is strongly influenced by the EoS. The GW170817 analysis for a $1.4M_\odot$ NS (Abbott et al., 2017) gave an upper limit of $\Lambda < 800$, which was later improved to $\Lambda = 190^{+390}_{-120}$ (Abbott et al., 2018).

From Table 1, we notice that most of the adopted EoSs in this work are compatible with the nuclear empirical values, the NS maximum mass, and the tidal deformability of a 1.4 $M_\odot$ NS. We, therefore, consider this set of EoSs for the analysis of the neutron skin thickness, which is discussed in the following Section 4.

3 Constraints on the nuclear EoS

An important check for the EoS is the behaviour of the symmetry energy slope L vs. S_0, and this is plotted in Figure 1. The full green triangles represent the microscopic calculations (left panel), whereas the phenomenological ones are shown in the right panel. The experimental constraints indicate those derived from the study of isospin diffusion in heavy ion collisions (HIC, blue band) (Tsang et al., 2009); the electric dipole polarizability (violet band) (Roca-Maza et al., 2015); the neutron skin thickness in Sn isotopes (orange band) (Chen et al., 2010); the finite-range droplet mass model calculations (FRDM, magenta rectangle) (Möller et al., 2012); the isobaric analog state (IAS) phenomenology combined with the ^{208}Pb neutron-skin thickness (green band) (Danielewicz and Lee, 2014); the recent analysis of the PREX-II experiment (black cross) (Essick et al., 2021). The blue solid curve is the unitary gas bound (Tews et al., 2017): only values of (S_0, L) to the right

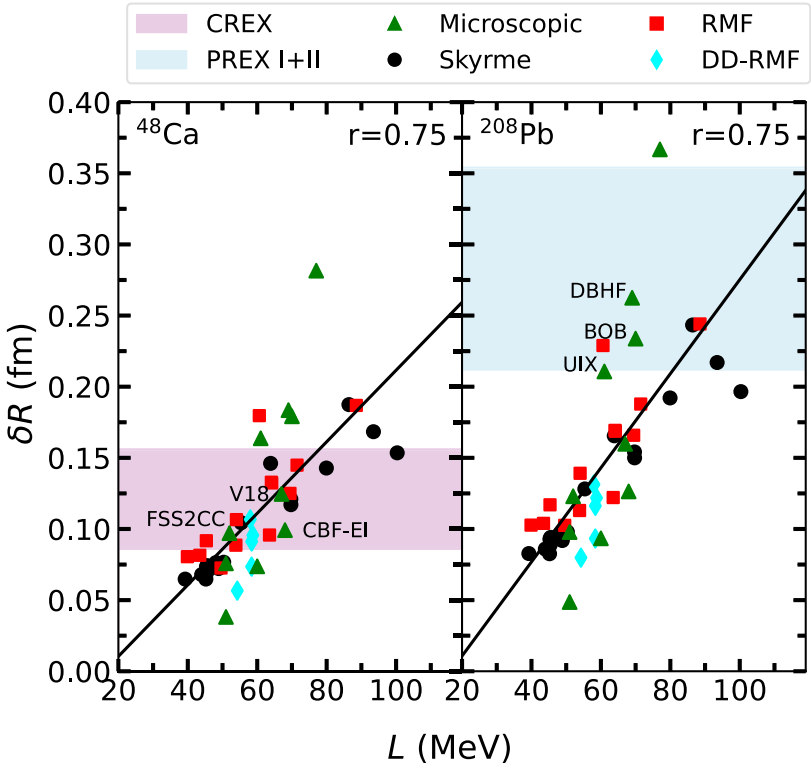

FIGURE 3
The neutron skin thickness for ^{48}Ca (left panel) and ^{208}Pb (right panel) is displayed as a function of L for the different EoS present in Table 1. The bands show the experimental constraints discussed in ref. (Adhikari et al., 2021; Adhikari et al., 2022). The solid lines indicate a linear fit of the EoS data. The values of the corresponding correlation factors r are also given.

of the curve are allowed. We see that all considered constraints are not simultaneously fulfilled in any area of the parameter space, probably because of the strong model dependencies in the extraction of the constraints from the raw data. Hence, at the moment, no theoretical models can be ruled out *a priori*, except those which are predicting values of the symmetry energy parameters outside the considered range.

A further important check regards the high-density behaviour of the nuclear symmetry energy, as illustrated in Ref. (Russotto et al., 2023). In the last few years several heavy-ion collisions experiments at relativistic energies have been performed in order to constrain the high-density symmetry energy. Figure 2 displays the ASY-EOS data (Russotto et al., 2016) (blue band) and the FOPI-LAND ones (Russotto et al., 2011) (light green band) as a function of the density, HIC (Sn + Sn) diffuseness measurements (Tsang et al., 2009) (grey band), whereas the red dashed contour labeled by IAS shows the results of Ref. (Danielewicz and Lee, 2014). For completeness, we also display the results of a Bayesian analysis (Tsang et al., 2024) which determines the boundaries at 68% (dark pink) and 95% confidence intervals (light pink) of the posterior distributions using an initial sample size of 3M of EoS. The experimental data are plotted up to $\rho = 2\rho_0$, and they all show a monotonically increasing behaviour with increasing density. In the four panels the symmetry energy is plotted vs. the nucleonic density for the microscopic models (upper left), for some of the Skyrme models (upper right), RMF models (lower left), and DD-RMF models (lower right) listed in Table 1. Except a couple of cases, i.e., BSk26 and SLy10, all EoS agree with the experimental data and the Bayesian analysis, thus confirming the need of more accurate experiments in order to disentangle the various theoretical approaches.

4 The neutron skin thickness

The strong correlation between the neutron skin thickness and the slope parameter L at normal nuclear saturation density was shown first by Brown and Typel (Brown, 2000; Typel and Brown, 2001), and confirmed later by other authors (Steiner et al., 2005; Centelles et al., 2009; Horowitz and Piekarewicz, 2001; Horowitz et al., 2001; Furnstahl, 2002). A measurement of the thickness allows to establish an empirical calibration point for the pressure of neutron star matter at subnuclear densities, and coupled with a NS radius measurement could determine the pressure at supranuclear densities. In fact, the neutron skin thickness and the NS size originate both from the pressure of neutron-rich matter, hence are sensitive to the same EoS. Therefore, the Typel-Brown correlation would be helpful in establishing the pressure–density relationship over a wide range of densities inside neutron stars.

The neutron skin thickness can be defined as the difference between the neutron (R_n) and proton (R_p) root-mean-square radii: $\delta R = \sqrt{\langle r_n^2 \rangle} - \sqrt{\langle r_p^2 \rangle}$. Since the microscopic approaches discussed before are not suited for the description of finite nuclei, we prefer to

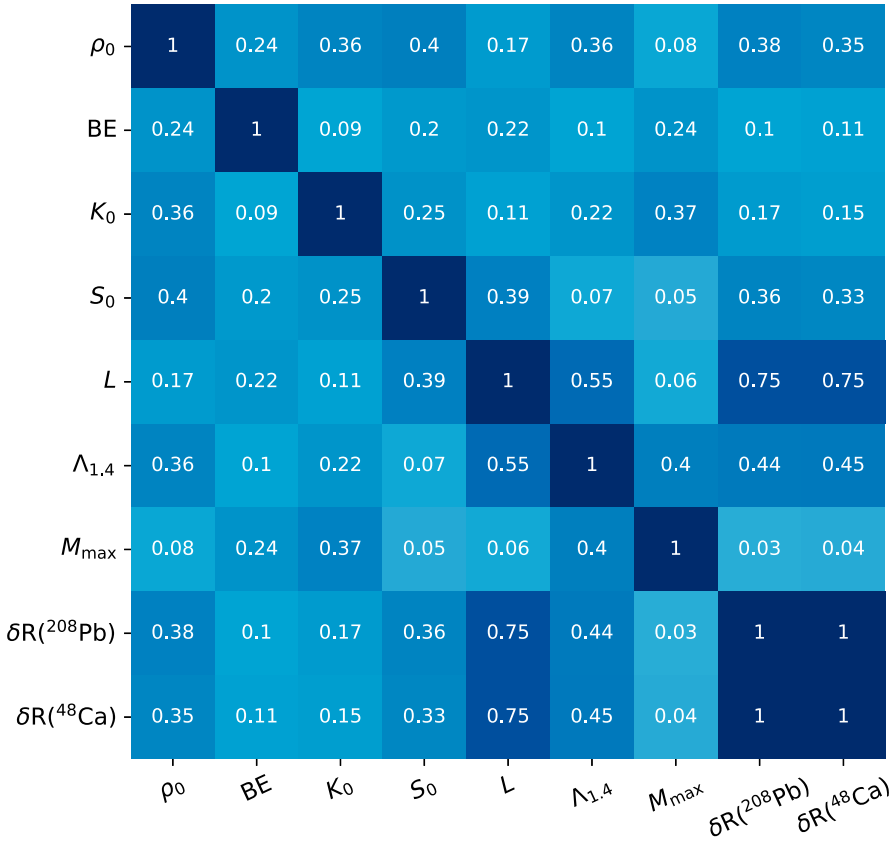

FIGURE 4
The correlation matrix between nuclear saturation properties and NS properties for the EoS ensemble shown in Table 1.

use a different approach based on Ref. (Vidaña et al., 2009), in which an estimation of the neutron skin thickness of ^{208}Pb and ^{132}Sn was made following the suggestion of Ref. (Steiner et al., 2005). In this case δR is calculated to lowest order in the diffuseness corrections as $\delta R \sim \sqrt{\frac{3}{5}}t$, being t the thickness of semi-infinite asymmetric nuclear matter

$$t = \frac{\delta_c}{\rho_0(\delta_c)\left(1-\delta_c^2\right)} \frac{E_s}{4\pi r_0^2} \frac{\int_0^{\rho_0(\delta_c)} \rho^{1/2}\left[S_0/E_{sym}(\rho)-1\right]\left[E_{SNM}(\rho)-E_0\right]^{-1/2} d\rho}{\int_0^{\rho_0(\delta_c)} \rho^{1/2}\left[E_{SNM}(\rho)-E_0\right]^{1/2} d\rho}. \tag{8}$$

In that expression, E_s is the surface energy taken from the semi-empirical mass formula equal to 17.23 MeV, r_0 is obtained from the normalization condition $(4\pi r_0^3/3)(0.16) = 1$, and δ_c is the isospin asymmetry in the center of the nucleus taken as $\delta_c = \delta/2$ according to Thomas-Fermi calculations. For consistency, we use this same method also for calculating the thickness in the phenomenological approaches. In Figure 3, we show the results of our calculations and compare them with experimental bands regarding CREX (left panel, magenta) and PREX I + II (right panel, cyan). Those experiments yield for PREX I + II a neutron skin thickness δR(^{208}Pb) = 0.283 ± 0.071 fm, whereas the measurement of the neutron skin of ^{48}Ca with the same technique gives smaller values, i.e., δR(^{48}Ca) = 0.121 ± 0.035 fm, thus pushing L towards larger or smaller values respectively. Data are shown as a function of the parameter L. The linear increase of δR with L is not surprising because the neutron skin thickness in heavy nuclei is determined by the pressure difference between neutrons and protons, and this is proportional to the parameter L, that is, $P(\rho_0, \delta) \approx L\rho_0\delta^2/3$. We notice that the theoretical predictions show some correlation between δR and L, as indicated by the linear fits (solid line) and by the value of the correlation coefficient, $r = 0.75$, in both cases. This is slightly smaller than the previous result shown in ref. (Burgio and Vidaña, 2020), where the chosen EoS set was not filtered with respect to the NS observational data. It has to be noticed that, in both cases, the microscopic calculations alone seem to lie on a curve with a slope different than the one of the phenomenological calculations. However, due to the small number of points available for the microscopic approaches, no firm conclusion can be drawn. We also notice that the same EoS is unable to reproduce both the CREX and PREX I + II data; for instance, among the microscopic approaches, the CREX data set is well reproduced by the FSS2CC, V18, and CBF-EI models, whereas DBHF, BOB, and UIX fall in the range of PREX I + II. Those EoS differ not only by the many-body technique adopted, but also by the nucleon-nucleon interaction. A similar behavior can also be found for the phenomenological models such as Rs, SkT4, BSR8, and GL97 respectively. This might indicate a possible tension

between the experimental data and the current understanding of the EoS. Though, it has to be stressed that the present calculations of the neutron skin thickness are based on the concept of semi-infinite nuclear matter (see Equation 8), which could be inappropriate. However, a similar result has already been found in other works, using suitable methods for finite nuclei (Lattimer, 2023). Further laboratory experiments on medium size nuclei, or a re-analysis of the current data could help to clarify this point.

Finally, in Figure 4, we display a correlation matrix among the saturation properties shown in Table 1, with $\Lambda_{1.4}$, $M_{\max}$ and the neutron skin thickness for ^{48}Ca and ^{208}Pb. The matrix confirms the weak correlation of δR with the L parameter already shown in Figure 3. A weaker degree of correlation is found between $\Lambda_{1.4}$ and L (r = 0.55), whereas no evident correlation between $\Lambda_{1.4}$ and S_0 and K_0 is found.

5 Conclusions

In this work, we have analyzed the predictions of microscopic and phenomenological EoS for the neutron skin thickness δR of ^{48}Ca and ^{208}Pb, and compared with the recent experimental data, CREX and PREX I + II. We have used an ensemble of different EoS models, that includes microscopic calculations based on the (Dirac)Brueckner–Hartree–Fock theory, the variational method, and Quantum Monte Carlo techniques, as well as several phenomenological Skyrme, and RMF models. The chosen EoSs are compatible with the constraints imposed by laboratory data on saturation properties of finite nuclei, and observational data by NICER and GW170817 regarding the NS mass and $\Lambda_{1.4}$.

We have found a linear correlation between the neutron skin thickness δR of ^{48}Ca and ^{208}Pb and the L parameter, as already pointed out by several authors using nonrelativistic and relativistic phenomenological models. A weaker linear correlation with the tidal deformability $\Lambda_{1.4}$ is evident.

The most important result of our analysis is that the same EoS cannot reproduce at the same time the CREX and PREX I + II experimental data. Therefore, those measurements do not allow us to select the most compatible EoS among the ones considered in this work. Future NS observations, along with planned experiments in existing facilities or in next-generation radioactive ion beam laboratories, are fundamental to provide more stringent constraints on the nuclear EoS, thus finally improving our knowledge of the extreme density matter conditions.

Data availability statement

The raw data supporting the conclusions of this article will be made available by the authors, without undue reservation.

Author contributions

GFB: Conceptualization, Methodology, Validation, Writing–original draft, Writing–review and editing. HCD: Software, Validation, Visualization, Writing–review and editing. IV: Conceptualization, Methodology, Software, Validation, Writing–review and editing.

Funding

The author(s) declare that no financial support was received for the research, authorship, and/or publication of this article.

Conflict of interest

The authors declare that the research was conducted in the absence of any commercial or financial relationships that could be construed as a potential conflict of interest.

The author(s) declared that they were an editorial board member of Frontiers, at the time of submission. This had no impact on the peer review process and the final decision.

Generative AI statement

The author(s) declare that no Generative AI was used in the creation of this manuscript.

Publisher's note

All claims expressed in this article are solely those of the authors and do not necessarily represent those of their affiliated organizations, or those of the publisher, the editors and the reviewers. Any product that may be evaluated in this article, or claim that may be made by its manufacturer, is not guaranteed or endorsed by the publisher.

References

Abbott, B., Abbott, R., Abbott, T., Acernese, F., Ackley, K., Adams, C., et al. (2017). GW170817: observation of gravitational waves from a binary neutron star inspiral. *Phys. Rev. Lett.* 119, 161101. doi:10.1103/PhysRevLett.119.161101

Abbott, B. P., Abbott, R., Abbott, T., Acernese, F., Ackley, K., Adams, C., et al. (2018). GW170817: measurements of neutron star radii and equation of state. *Phys. Rev. Lett.* 121, 161101. doi:10.1103/PhysRevLett.121.161101

Abbott, B. P., Abbott, R., Abbott, T., Acernese, F., Ackley, K., Adams, C., et al. (2019). Properties of the binary neutron star merger GW170817. *Phys. Rev. X* 9, 011001. doi:10.1103/PhysRevX.9.011001

Adhikari, D., Albataineh, H., Androic, D., Aniol, K., Armstrong, D., Averett, T., et al. (2021). Accurate determination of the neutron skin thickness of ^{208}Pb through parity-violation in electron scattering. *Phys. Rev. Lett.* 126, 172502. doi:10.1103/PhysRevLett.126.172502

Adhikari, D., Albataineh, H., Androic, D., Aniol, K., Armstrong, D., Averett, T., et al. (2022). Precision determination of the neutral weak form factor of ^{48}Ca. *Phys. Rev. Lett.* 129, 042501. doi:10.1103/PhysRevLett.129.042501

Akmal, A., Pandharipande, V. R., and Ravenhall, D. G. (1998). Equation of state of nucleon matter and neutron star structure. *Phys. Rev. C* 58, 1804–1828. doi:10.1103/PhysRevC.58.1804

Antoniadis, J., Freire, P. C. C., Wex, N., Tauris, T. M., Lynch, R. S., van Kerkwijk, M. H., et al. (2013). A massive pulsar in a compact relativistic binary. *Science* 340, 6131. doi:10.1126/science.1233232

Audi, G., Wapstra, A. H., and Thibault, C. (2003). The Ame2003 atomic mass evaluation. *Nucl. Phys. A* 729, 337–676. doi:10.1016/j.nuclphysa.2003.11.003

Baldo, M. (1999) "Nuclear methods and the nuclear equation of state," in *International review of nuclear physics*, 8. Singapore: World Scientific. doi:10.1142/2657

Baldo, M., Bombaci, I., and Burgio, G. F. (1997). Microscopic nuclear equation of state with three-body forces and neutron star structure. *Astron. Astrophys.* 328, 274–282. doi:10.48550/arXiv.astro-ph/9707277

Baldo, M., and Burgio, G. F. (2016). The nuclear symmetry energy. *Prog. Part. Nucl. Phys.* 91, 203–258. doi:10.1016/j.ppnp.2016.06.006

Baldo, M., and Fukukawa, K. (2014). Nuclear matter from effective quark-quark interaction. *Phys. Rev. Lett.* 113, 242501. doi:10.1103/PhysRevLett.113.242501

Baym, G., Pethick, C., and Sutherland, P. (1971). The Ground state of matter at high densities: equation of state and stellar models. *Astrophys. J.* 170, 299–317. doi:10.1086/151216

Benhar, O., and Lovato, A. (2017). Perturbation theory of nuclear matter with a microscopic effective interaction. *Phys. Rev. C* 96, 054301. doi:10.1103/PhysRevC.96.054301

Boguta, J., and Bodmer, A. R. (1977). Relativistic calculation of nuclear matter and the nuclear surface. *Nucl. Phys. A* 292, 413–428. doi:10.1016/0375-9474(77)90626-1

Brown, B. A. (2000). Neutron radii in nuclei and the neutron equation of state. *Phys. Rev. Lett.* 85, 5296–5299. doi:10.1103/PhysRevLett.85.5296

Burgio, G., Schulze, H.-J., Vidaña, I., and Wei, J.-B. (2021). Neutron stars and the nuclear equation of state. *Prog. Part. Nucl. Phys.* 120, 103879. doi:10.1016/j.ppnp.2021.103879

Burgio, G. F., and Fantina, A. F. (2018). Nuclear equation of state for compact stars and supernovae. *Astrophys. Space Sci.Libr.* 457, 255–335. doi:10.1007/978-3-319-97616-7_6

Burgio, G. F., and Vidaña, I. (2020). The equation of state of nuclear matter: from finite nuclei to neutron stars. *Universe* 6, 119. doi:10.3390/universe6080119

Carbone, A., Colò, G., Bracco, A., Cao, L.-G., Bortignon, P. F., Camera, F., et al. (2010). Constraints on the symmetry energy and neutron skins from pygmy resonances in ^{68}Ni and ^{132}Sn. *Phys. Rev. C* 81, 041301. doi:10.1103/PhysRevC.81.041301

Centelles, M., Roca-Maza, X., Viñas, X., and Warda, M. (2009). Nuclear symmetry energy probed by neutron skin thickness of nuclei. *Phys. Rev. Lett.* 102, 122502. doi:10.1103/PhysRevLett.102.122502

Chabanat, E. (1995). Universitè Claude Bernard Lyon-1. *Rep. No. LYCENT 9501*.

Chabanat, E., Bonche, P., Haensel, P., Meyer, J., and Schaeffer, R. (1997). A Skyrme parametrization from subnuclear to neutron star densities. *Nucl. Phys. A* 627, 710–746. doi:10.1016/S0375-9474(97)00596-4

Chabanat, E., Bonche, P., Haensel, P., Meyer, J., and Schaeffer, R. (1998). A Skyrme parametrization from subnuclear to neutron star densitiesPart II. Nuclei far from stabilities. *Nucl. Phys. A* 635, 231–256. doi:10.1016/S0375-9474(98)00180-8

Chen, L.-W., Ko, C. M., Li, B.-A., and Xu, J. (2010). Density slope of the nuclear symmetry energy from the neutron skin thickness of heavy nuclei. *Phys. Rev. C* 82, 024321. doi:10.1103/PhysRevC.82.024321

Chen, W.-C., and Piekarewicz, J. (2015). Searching for isovector signatures in the neutron-rich oxygen and calcium isotopes. *Phys. Lett. B* 748, 284–288. doi:10.1016/j.physletb.2015.07.020

Colò, G., van Giai, N., Meyer, J., Bennaceur, K., and Bonche, P. (2004). Microscopic determination of the nuclear incompressibility within the nonrelativistic framework. *Phys. Rev. C* 70, 024307. doi:10.1103/PhysRevC.70.024307

Cromartie, H. T., Fonseca, E., Ransom, S. M., Demorest, P. B., Arzoumanian, Z., Blumer, H., et al. (2019). Relativistic shapiro delay measurements of an extremely massive millisecond pulsar. *Nat. Astron.* 4, 72–76. doi:10.1038/s41550-019-0880-2

Danielewicz, P., and Lee, J. (2014). Symmetry energy II: isobaric analog states. *Nucl. Phys. A* 922, 1–70. doi:10.1016/j.nuclphysa.2013.11.005

Das, H. C., Kumar, A., Kumar, B., Biswal, S. K., and Patra, S. K. (2021). BigApple force and its implications to finite nuclei and astrophysical objects. *Int. J. Mod. Phys. E* 30, 2150088. doi:10.1142/S0218301321500889

Demorest, P. B., Pennucci, T., Ransom, S. M., Roberts, M. S., and Hessels, J. W. (2010). A two-solar-mass neutron star measured using shapiro delay. *Nature* 467, 1081–1083. doi:10.1038/nature09466

de Vries, H., de Jager, C. W., and de Vries, C. (1987). Nuclear charge-density-distribution parameters from elastic electron scattering. *Atomic Data Nucl. Data Tables* 36, 495–536. doi:10.1016/0092-640X(87)90013-1

Dhiman, S. K., Kumar, R., and Agrawal, B. K. (2007). Nonrotating and rotating neutron stars in the extended field theoretical model. *Phys. Rev. C* 76, 045801. doi:10.1103/PhysRevC.76.045801

Essick, R., Tews, I., Landry, P., and Schwenk, A. (2021). Astrophysical constraints on the symmetry energy and the neutron skin of ^{208}Pb with minimal modeling assumptions. *Phys. Rev. Lett.* 127, 192701. doi:10.1103/PhysRevLett.127.192701

Fattoyev, F. J., Horowitz, C. J., Piekarewicz, J., and Reed, B. (2020). GW190814: impact of a 2.6 solar mass neutron star on the nucleonic equations of state. *Phys. Rev. C* 102, 065805. doi:10.1103/PhysRevC.102.065805

Fattoyev, F. J., and Piekarewicz, J. (2010). Relativistic models of the neutron-star matter equation of state. *Phys. Rev. C* 82, 025805. doi:10.1103/PhysRevC.82.025805

Feynman, R. P., Metropolis, N., and Teller, E. (1949). Equations of state of elements based on the generalized Fermi-Thomas theory. *Phys. Rev.* 75, 1561–1573. doi:10.1103/PhysRev.75.1561

Flanagan, E. E., and Hinderer, T. (2008). Constraining neutron star tidal Love numbers with gravitational wave detectors. *Phys. Rev. D.* 77, 021502. doi:10.1103/PhysRevD.77.021502

Fonseca, E., Pennucci, T. T., Ellis, J. A., Stairs, I. H., Nice, D. J., Ransom, S. M., et al. (2016). The NANOGrav nine-year data set: mass and geometric measurements of binary millisecond pulsars. *Astrophys. J.* 832, 167. doi:10.3847/0004-637X/832/2/167

Fuchs, C., Faessler, A., Zabrodin, E., and Zheng, Y.-M. (2001). Probing the nuclear equation of state by production in heavy-ion collisions. *Phys. Rev. Lett.* 86, 1974–1977. doi:10.1103/PhysRevLett.86.1974

Fukukawa, K., Baldo, M., Burgio, G. F., Lo Monaco, L., and Schulze, H.-J. (2015). Nuclear matter equation of state from a quark-model nucleon-nucleon interaction. *Phys. Rev. C* 92, 065802. doi:10.1103/PhysRevC.92.065802

Furnstahl, R. J. (2002). Neutron radii in mean-field models. *Nucl. Phys. A* 706, 85–110. doi:10.1016/S0375-9474(02)00867-9

Gandolfi, S., Illarionov, A. Y., Fantoni, S., Miller, J. C., Pederiva, F., and Schmidt, K. E. (2010). Microscopic calculation of the equation of state of nuclear matter and neutron star structure. *Mon. Not. Roy. Astron. Soc.* 404, L35–L39. doi:10.1111/j.1745-3933.2010.00829.x

Goriely, S., Chamel, N., and Pearson, J. M. (2013). Further explorations of skyrme-Hartree-Fock-bogoliubov mass formulas. xiii. the 2012 atomic mass evaluation and the symmetry coefficient. *Phys. Rev. C* 88, 024308. doi:10.1103/PhysRevC.88.024308

Grangé, P., Lejeune, A., Martzolff, M., and Mathiot, J.-F. (1989). Consistent three-nucleon forces in the nuclear many-body problem. *Phys. Rev. C* 40, 1040–1060. doi:10.1103/PhysRevC.40.1040

Gross-Boelting, T., Fuchs, C., and Faessler, A. (1999). Covariant representations of the relativistic Brueckner T-matrix and the nuclear matter problem. *Nucl. Phys. A* 648, 105–137. doi:10.1016/S0375-9474(99)00022-6

Guillot, S., Servillat, M., Webb, N. A., and Rutledge, R. E. (2013). Measurement of the radius of neutron stars with high signal-to-noise quiescent low-mass x-ray binaries in globular clusters. *Astrophys. J.* 772, 7. doi:10.1088/0004-637X/772/1/7

Hartle, J. B. (1967). Slowly rotating relativistic stars. I. Equations of structure. *Astrophys. J.* 150, 1005–1029. doi:10.1086/149400

Hinderer, T. (2008). Tidal Love numbers of neutron stars. *Astrophys. J.* 677, 1216–1220. doi:10.1086/533487

Hinderer, T. (2009). Erratum: "Tidal Love numbers of neutron stars" (2008, ApJ, 677, 1216). *Astrophys. J.* 697, 964. doi:10.1088/0004-637X/697/1/964

Hinderer, T., Lackey, B. D., Lang, R. N., and Read, J. S. (2010). Tidal deformability of neutron stars with realistic equations of state and their gravitational wave signatures in binary inspiral. *Phys. Rev. D.* 81, 123016. doi:10.1103/PhysRevD.81.123016

Horowitz, C. J., and Piekarewicz, J. (2001). Neutron star structure and the neutron radius of ^{208}Pb. *Phys. Rev. Lett.* 86, 5647–5650. doi:10.1103/PhysRevLett.86.5647

Horowitz, C. J., Pollock, S. J., Souder, P. A., and Michaels, R. (2001). Parity violating measurements of neutron densities. *Phys. Rev. C* 63, 025501. doi:10.1103/PhysRevC.63.025501

Klimkiewicz, A., Paar, N., Adrich, P., Fallot, M., Boretzky, K., Aumann, T., et al. (2007). Nuclear symmetry energy and neutron skins derived from pygmy dipole resonances. *Phys. Rev. C* 76, 051603. doi:10.1103/PhysRevC.76.051603

Kumar, B., Patra, S. K., and Agrawal, B. K. (2018). New relativistic effective interaction for finite nuclei, infinite nuclear matter, and neutron stars. *Phys. Rev. C* 97, 045806. doi:10.1103/PhysRevC.97.045806

Kumar, B., Singh, S. K., Agrawal, B. K., and Patra, S. K. (2017). New parameterization of the effective field theory motivated relativistic mean field model. *Nucl. Phys. A* 966, 197–207. doi:10.1016/j.nuclphysa.2017.07.001

Kumar, R., Agrawal, B. K., and Dhiman, S. K. (2006). Effects of omega meson self-coupling on the properties of finite nuclei and neutron stars. *Phys. Rev. C* 74, 034323. doi:10.1103/PhysRevC.74.034323

Lattimer, J. M. (2012). The nuclear equation of state and neutron star masses. *Ann. Rev. Nucl. Sci.* 62, 485–515. doi:10.1146/annurev-nucl-102711-095018

Lattimer, J. M. (2023). Constraints on nuclear symmetry energy parameters. *Particles* 6, 30–56. doi:10.3390/particles6010003

Li, B.-An, Ramos, À., Verde, G., and Vidaña, I. (2014). Topical issue on nuclear symmetry energy. *Eur. Phys. J.* 50, 9. doi:10.1140/epja/i2014-14009-x

Li, Z. H., Lombardo, U., Schulze, H.-J., and Zuo, W. (2008). Consistent nucleon-nucleon potentials and three-body forces. *Phys. Rev. C* 77, 034316. doi:10.1103/PhysRevC.77.034316

Li, Z. H., and Schulze, H. J. (2008). Neutron star structure with modern nucleonic three-body forces. *Phys. Rev. C* 78, 028801. doi:10.1103/PhysRevC.78.028801

Machleidt, R. (1989). The Meson theory of nuclear forces and nuclear structure. *Adv. Nucl. Phys.* 19, 189–376. doi:10.1007/978-1-4613-9907-0

Machleidt, R., Holinde, K., and Elster, C. (1987). The Bonn meson exchange model for the nucleon nucleon interaction. *Phys. Rep.* 149, 1–89. doi:10.1016/S0370-1573(87)80002-9

Margueron, J., Hoffmann Casali, R., and Gulminelli, F. (2018). Equation of state for dense nucleonic matter from metamodeling. I. Foundational aspects. *Phys. Rev. C* 97, 025805. doi:10.1103/PhysRevC.97.025805

Miller, M. C., Lamb, F. K., Dittmann, A. J., Bogdanov, S., Arzoumanian, Z., Gendreau, K. C., et al. (2019). PSR J0030+0451 mass and radius from NICER data and implications for the properties of neutron star matter. *Astrophys. J. Lett.* 887, L24. doi:10.3847/2041-8213/ab50c5

Möller, P., Myers, W. D., Sagawa, H., and Yoshida, S. (2012). New finite-range droplet mass model and equation-of-state parameters. *Phys. Rev. Lett.* 108, 052501. doi:10.1103/PhysRevLett.108.052501

Mondal, C., Agrawal, B. K., De, J. N., and Samaddar, S. K. (2016). Sensitivity of elements of the symmetry energy of nuclear matter to the properties of neutron-rich systems. *Phys. Rev. C* 93, 044328. doi:10.1103/PhysRevC.93.044328

Nagels, M. M., Rijken, T. A., and de Swart, J. J. (1978). Low-energy nucleon-nucleon potential from Regge-pole theory. *Phys. Rev. D.* 17, 768–776. doi:10.1103/PhysRevD.17.768

Negele, J. W., and Vautherin, D. (1973). Neutron star matter at subnuclear densities. *Nucl. Phys. A* 207, 298–320. doi:10.1016/0375-9474(73)90349-7

Nikšić, T., Vretenar, D., Finelli, P., and Ring, P. (2002). Relativistic Hartree-Bogoliubov model with density-dependent meson-nucleon couplings. *Phys. Rev. C* 66, 024306. doi:10.1103/PhysRevC.66.024306

Oertel, M., Hempel, M., Klähn, T., and Typel, S. (2017). Equations of state for supernovae and compact stars. *Rev. Mod. Phys.* 89, 015007. doi:10.1103/RevModPhys.89.015007

Özel, F., and Freire, P. (2016). Masses, radii, and the equation of state of neutron stars. *Ann. Rev. Astron. Astrophys.* 54, 401–440. doi:10.1146/annurev-astro-081915-023322

Piekarewicz, J. (2004). Unmasking the nuclear matter equation of state. *Phys. Rev. C* 69, 041301. doi:10.1103/PhysRevC.69.041301

Piekarewicz, J. (2010). Do we understand the incompressibility of neutron-rich matter? *J. Phys. G Nucl. Phys.* 37, 064038. doi:10.1088/0954-3899/37/6/064038

Potekhin, A. Y., Fantina, A. F., Chamel, N., Pearson, J. M., and Goriely, S. (2013). Analytical representations of unified equations of state for neutron-star matter. *Astronomy and Astrophysics* 560, A48. doi:10.1051/0004-6361/201321697

Pudliner, B. S., Pandharipande, V. R., Carlson, J., Pieper, S. C., and Wiringa, R. B. (1997). Quantum Monte Carlo calculations of nuclei with A<~7. *Phys. Rev. C* 56, 1720–1750. doi:10.1103/PhysRevC.56.1720

Pudliner, B. S., Pandharipande, V. R., Carlson, J., and Wiringa, R. B. (1995). Quantum Monte Carlo calculations of A<~6 nuclei. *Phys. Rev. Lett.* 74, 4396–4399. doi:10.1103/PhysRevLett.74.4396

Radice, D., Perego, A., Zappa, F., and Bernuzzi, S. (2018). GW170817: joint constraint on the neutron star equation of state from multimessenger observations. *Astrophys. J.* 852, L29. doi:10.3847/2041-8213/aaa402

Reed, B. T., Fattoyev, F. J., Horowitz, C. J., Piekarewicz, J., Armstrong, D. S., Averett, T., et al. (2021). Accurate determination of the neutron skin thickness of ^{208}Pb through parity-violation in electron scattering. *Phys. Rev. Lett.* 126, 172502. doi:10.1103/PhysRevLett.126.172502

Riley, T. E., Watts, A. L., Bogdanov, S., Ray, P. S., Ludlam, R. M., Guillot, S., et al. (2019). A NICER view of PSR J0030+0451: millisecond pulsar parameter estimation. *Astrophys. J. Lett.* 887, L21. doi:10.3847/2041-8213/ab481c

Roca-Maza, X., Viñas, X., Centelles, M., Agrawal, B. K., Colò, G., Paar, N., et al. (2015). Neutron skin thickness from the measured electric dipole polarizability in ^{68}Ni^{120}Sn and ^{208}Pb. *Phys. Rev. C* 92, 064304. doi:10.1103/PhysRevC.92.064304

Romani, R. W., Kandel, D., Filippenko, A. V., Brink, T. G., and Zheng, W. (2022). PSR J0952-0607: the fastest and heaviest known galactic neutron star. *Astrophys. J. Lett.* 934, L17. doi:10.3847/2041-8213/ac8007

Routaray, P., Mohanty, S. R., Das, H. C., Ghosh, S., Kalita, P. J., Parmar, V., et al. (2023). Investigating dark matter-admixed neutron stars with NITR equation of state in light of PSR J0952-0607. *J. Cosmol. Astropart. Phys.* 2023, 073. doi:10.1088/1475-7516/2023/10/073

Russotto, P., Cozma, M. D., De Filippo, E., Le Fèvre, A., Leifels, Y., and Łukasik, J. (2023). Studies of the equation-of-state of nuclear matter by heavy-ion collisions at intermediate energy in the multi-messenger era: a review focused on GSI results. *La Riv. del Nuovo Cimento* 46, 1–70. doi:10.1007/s40766-023-00039-4

Russotto, P., Gannon, S., Kupny, S., Lasko, P., Acosta, L., Adamczyk, M., et al. (2016). Results of the ASY-EOS experiment at GSI: the symmetry energy at suprasaturation density. *Phys. Rev. C* 94, 034608. doi:10.1103/PhysRevC.94.034608

Russotto, P., Wu, P., Zoric, M., Chartier, M., Leifels, Y., Lemmon, R., et al. (2011). Symmetry energy from elliptic flow in ^{197}Au + ^{197}Au. *Phys. Lett. B* 697, 471–476. doi:10.1016/j.physletb.2011.02.033

Salmi, T., Julia, S., Deneva, S., Ray, P. S., Watts, A. L., and Choudhury, D. (2024). A NICER view of PSR j1231-1411: a complex case. *arXiv:2409*. doi:10.48550/arXiv.2409.14923

Shlomo, S., Kolomietz, V. M., and Colò, G. (2006). Deducing the nuclear-matter incompressibility coefficient from data on isoscalar compression modes. *EPJA* 30, 23–30. doi:10.1140/epja/i2006-10100-3

Steiner, A. W., Prakash, M., Lattimer, J. M., and Ellis, P. J. (2005). Isospin asymmetry in nuclei and neutron stars. *Phys. Rep.* 411, 325–375. doi:10.1016/j.physrep.2005.02.004

Stoks, V. G. J., Klomp, R. A. M., Terheggen, C. P. F., and de Swart, J. J. (1994). Construction of high quality N N potential models. *Phys. Rev. C* 49, 2950–2962. doi:10.1103/PhysRevC.49.2950

Stone, J. R., and Reinhard, P. G. (2007). The Skyrme interaction in finite nuclei and nuclear matter. *Prog. Part. Nucl. Phys.* 58, 587–657. doi:10.1016/j.ppnp.2006.07.001

Sulaksono, A., and Mart, T. (2006). Low density instability in relativistic mean field models. *Phys. Rev. C* 74, 045806. doi:10.1103/PhysRevC.74.045806

Tews, I., Lattimer, J. M., Ohnishi, A., and Kolomeitsev, E. E. (2017). Symmetry parameter constraints from a lower bound on neutron-matter energy. *Astrophys. J.* 848, 105. doi:10.3847/1538-4357/aa8db9

Tsang, C. Y., Tsang, M. B., Lynch, W. G., Kumar, R., and Horowitz, C. J. (2024). Determination of the equation of state from nuclear experiments and neutron star observations. *Nat. Astron.* 8, 328–336. doi:10.1038/s41550-023-02161-z

Tsang, M. B., Zhang, Y., Danielewicz, P., Famiano, M., Li, Z., Lynch, W. G., et al. (2009). Constraints on the density dependence of the symmetry energy. *Phys. Rev. Lett.* 102, 122701. doi:10.1103/PhysRevLett.102.122701

Typel, S., and Brown, B. A. (2001). Neutron radii and the neutron equation of state in relativistic models. *Phys. Rev. C* 64, 027302. doi:10.1103/PhysRevC.64.027302

Typel, S., and Wolter, H. H. (1999). Relativistic mean field calculations with density-dependent meson-nucleon coupling. *Nucl. Phys. A* 656, 331–364. doi:10.1016/S0375-9474(99)00310-3

Vautherin, D., and Brink, D. M. (1972). Hartree-Fock calculations with Skyrme's interaction. I. Spherical nuclei. *Phys. Rev. C* 5, 626–647. doi:10.1103/PhysRevC.5.626

Vidaña, I., Providência, C., Polls, A., and Rios, A. (2009). Density dependence of the nuclear symmetry energy: a microscopic perspective. *Phys. Rev. C* 80, 045806. doi:10.1103/PhysRevC.80.045806

Wiringa, R. B., and Pieper, S. C. (2002). Evolution of nuclear spectra with nuclear forces. *Phys. Rev. Lett.* 89, 182501. doi:10.1103/PhysRevLett.89.182501

Wiringa, R. B., Stoks, V. G. J., and Schiavilla, R. (1995). Accurate nucleon-nucleon potential with charge-independence breaking. *Phys. Rev. C* 51, 38–51. doi:10.1103/PhysRevC.51.38

Xia, C.-J., Maruyama, T., Li, A., Yuan Sun, B., Long, W.-H., and Zhang, Y.-X. (2022). Unified neutron star EOSs and neutron star structures in RMF models. *Commun. Theor. Phys.* 74, 095303. doi:10.1088/1572-9494/ac71fd

Yakovlev, D., and Pethick, C. (2004). Neutron star cooling. *Annu. Rev. Astronomy Astrophysics* 42, 169–210. doi:10.1146/annurev.astro.42.053102.134013

Zhang, N.-B., Cai, B.-J., Li, B.-A., Newton, W. G., and Xu, J. (2017). How tightly is nuclear symmetry energy constrained by unitary Fermi gas? *Nucl. Sci. Tech.* 28, 181. doi:10.1007/s41365-017-0336-2

Zuo, W., Lejeune, A., Lombardo, U., and Mathiot, J. F. (2002). Microscopic three-body force for asymmetric nuclear matter. *Eur. Phys. J.* 14, 469–475. doi:10.1140/epja/i2002-10031-y